Imaging of the Carpal Tunnel and Median Nerve

8

Akira M. Murakami, Andrew Kompel, Alda Cossi, O. Kenechi Nwawka, and Ali Guermazi

Introduction

Carpal tunnel syndrome (CTS) is the most common entrapment neuropathy of the upper limb, with an estimated prevalence that is reportedly as high as 5% of the general population [1]. CTS is primarily a clinical diagnosis, made by an accurate patient history and physical exam. Electrodiagnostic tests (EDTs) may be performed to support the diagnosis, to differentiate among alternative diagnoses, or to further evaluate the presence of thenar atrophy and/or persistent numbness. Diagnostic imaging, such as conventional radiography, computed tomography (CT), magnetic resonance imaging (MRI), and ultrasound, is not routinely utilized [2, 3]. Despite this, radiologic studies can provide valuable supplemental information to the clinical exam and EDTs that can impact patient care. Specifically, these modalities can identify clinically relevant variant anatomy or diagnose different causes of secondary CTS such as space-occupying lesions or conditions. In postoperative patients, imaging may be able to identify causes of refractory or recurrent symptoms such as perineural fibrosis or insufficient tunnel release.

Recent advances in the imaging techniques of MRI and ultrasound have allowed detailed imaging of the median nerve that can provide morphologic and metabolic information that was not previously available. In particular, ultrasound now has a similar sensitivity and specificity to EDT and thus is a potential noninvasive screening exam for CTS [4]. The developing use of ultrasound elastography may further advance this sensitivity. In addition, with an increasing number of wrist MRIs performed, an understanding of carpal tunnel anatomy and related CTS imaging findings is critical.

Anatomy

A detailed review of the wrist anatomy is beyond the scope of this chapter. However specific points of the anatomy that are relevant to imaging will be discussed. The deep concave border of the carpal tunnel is made up of the capitate, hamate, and triquetrum. As most imaging modalities effectively depict the tunnel in the axial plane, the walls of the tunnel are often

A.M. Murakami (✉) • A. Kompel • A. Cossi
A. Guermazi
Department of Radiology, Boston University School of Medicine, Boston Medical Center, 820 Harrison Ave, FGH Building, Boston, MA 02118, USA
e-mail: akira.murakami@bmc.org

O.K. Nwawka
Department of Radiology and Imaging, Hospital for Special Surgery, Weill Medical College of Cornell University, 535 East 70th Street, New York, NY 10021, USA

S.F.M. Duncan, R. Kakinoki (eds.), *Carpal Tunnel Syndrome and Related Median Neuropathies*, DOI 10.1007/978-3-319-57010-5_8

more readily recognized, particularly by ultrasound and radiography. On the lateral wall, there is the scaphoid and trapezium. On the medial wall, there is the pisiform and hamate hook. The roof of the tunnel is covered by a thick, ligamentous band known as the flexor retinaculum. Laterally, the retinaculum attaches to the tubercles of the scaphoid and trapezium, and medially it attaches to the pisiform and hook of the hamate [5, 6].

Most of the tunnel is occupied by the flexor tendons of the hand, which include four flexor digitorum profundus and four flexor digitorum superficialis tendons. The flexor pollicis longus tendon is located along the radial aspect of the tunnel. A common synovial tendon sheath invests the flexor digitorum profundus and superficialis tendons. A separate synovial tendon sheath invests the flexor pollicis longus tendon sheath [5–7]. The sheath can often be seen outlining the tendons particularly on MRI, and it can become more conspicuous on other modalities when synovitis is present.

Within the distal forearm, the median nerve can be found between the muscle bellies of the flexor digitorum profundus and flexor digitorum superficialis. As the nerve approaches the carpal tunnel, it gives off a small superficial palmar cutaneous branch that courses superficial to the flexor retinaculum to supply sensation to the thenar eminence. The nerve courses laterally, to enter the carpal tunnel lying superficial to the flexor pollicis longus and index finger flexor digitorum superficialis tendons. After exiting the carpal tunnel, the median nerve sends a primary motor branch to the abductor pollicis brevis muscle and additional branches to the opponens pollicis, the superficial head of the flexor pollicis brevis, and the first and second lumbricalis. Sensory branches at this point supply the medial thumb, index, middle, and lateral ring fingers [5–7].

Variant anatomy within the carpal tunnel is frequently seen on imaging. The median nerve can be bifid at the carpal tunnel inlet; prevalence in the general population can be as high as 26%. A persistent median artery of the forearm is an embryologic remnant accessory artery arising from the ulnar artery in the proximal forearm. Within the carpal tunnel, the artery courses along the ulnar margin of the median nerve and can be seen in up to 20% of cadaveric dissections. When associated with a bifid median nerve, the artery can course between the nerve divisions, either enveloped in a common epineurium or as separate structure [6]. Anomalous muscles within the carpal tunnel, such as an accessory flexor digitorum superficialis muscle belly, have been reported as infrequent causes of carpal tunnel syndrome [8].

Radiography/Computed Tomography

The role of radiography and computed tomography (CT) is limited, as both modalities depict soft tissue structures with relatively poor contrast compared to MRI and ultrasound. However, in certain scenarios, these modalities may play a complementary role. For example, mineralization and calcifications present in mass lesions or amyloid deposits within the carpal tunnel may appear as relatively nonspecific foci of hypointense MRI signal or bright/echogenic shadowing foci on ultrasound. Such lesions can readily be detected and distinguished on radiography and CT. In the setting of trauma, both modalities can identify fracture patterns within the wrist that can potentially create mass effect on the carpal tunnel.

In radiography, the carpal tunnel view is optimal. The forearm is pronated and placed on the film cassette with the patient dorsiflexing the hand by the fingertip, with the opposite hand. The central X-ray beam is angled approximately 25–30° and directed at the volar surface of the carpal bones (Fig. 8.1), displaying the carpal tunnel in the axial plane. While soft tissue contrast is limited by the modality, mineralization within the tissue can be accurately visualized within the carpal tunnel space. Additionally, fractures of the hook of the hamate (Fig. 8.2), pisiform, and trapezium are more conspicuous compared to the typically performed three view radiographs (frontal, oblique, and lateral).

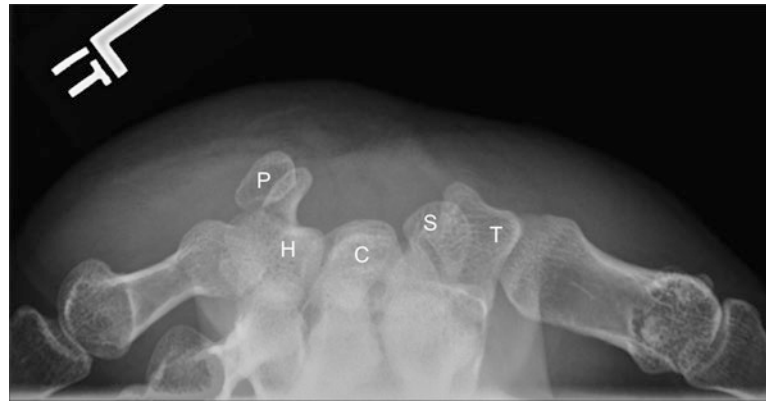

Fig. 8.1 Carpal tunnel view radiograph—normal anatomy; *P* pisiform, *H* hamate, *C* capitate, *S* scaphoid, *T* trapezium

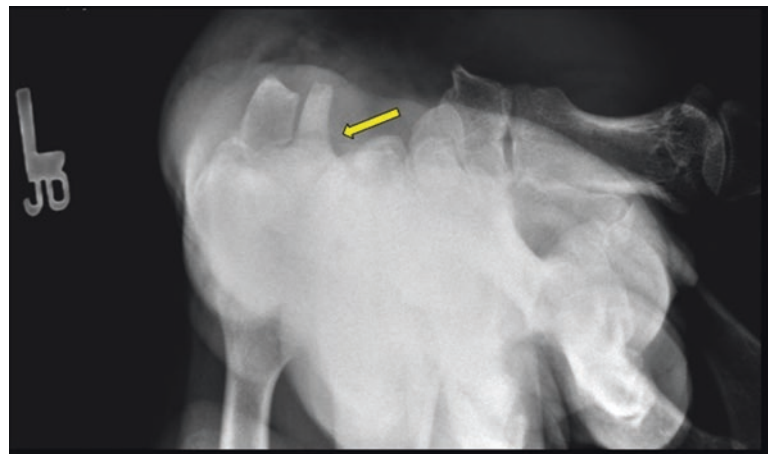

Fig. 8.2 Carpal tunnel view radiograph—fracture at the base of the hook of the hamate (*yellow arrow*)

Computed tomography (CT) has increased sensitivity for detecting soft tissue mineralization and fracture. The contours of mass lesions are more evident by cross-sectional imaging, but soft tissue contrast remains limited by the modality. The thin slice acquisition of multidetector array CT acquires isotropic data sets which allow multiplanar reformats to be created. These reformats increase the sensitivity for fracture (Fig. 8.3) and for space-occupying lesions within the carpal tunnel.

Magnetic Resonance Imaging

MRI depicts the carpal tunnel and potential pathology with high spatial resolution and soft tissue contrast. While imaging sequence protocols vary between institutions, the axial plane is frequently performed and highly diagnostic. Generally, a fluid-sensitive sequence such as a fast spin-echo proton density (PD) or T2-weighted sequence is utilized, depicting edema patterns as a bright or hyperintense signal. Because the nerve is small, edema signal can often be obscured by the surrounding fat; such sequences are thus often performed with fat suppression, making the signal more conspicuous. Commonly used methods of fat suppression are frequency-selective saturation of the fat resonance or a short tau recovery (STIR) [9]. Nonfat-saturated T1-weighted or fast spin-echo PD sequences are often included for anatomic detail of the tendons, median nerve, bone contour, and flexor retinaculum. While there is no particular standard matrix for carpal tunnel imaging, sequences on routine wrist evaluations can range from a matrix of 256 × 256 to as high as 512 × 256. Regardless of the matrix, the images

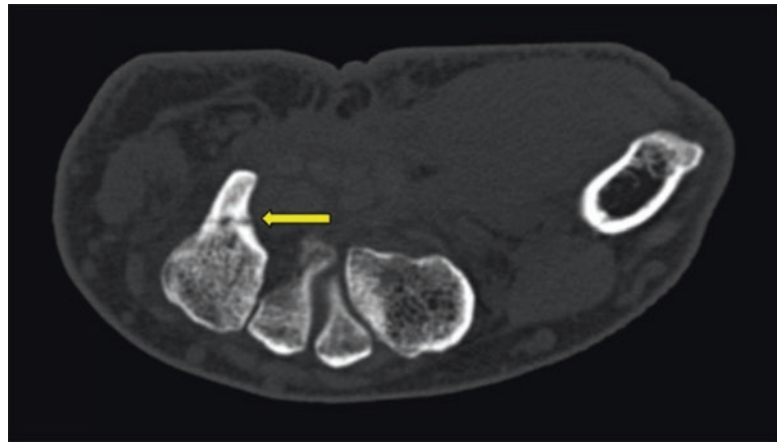

Fig. 8.3 Computed tomography axial image—fracture at the base of the hook of the hamate (*yellow arrow*)

must be able to display the overall morphology of the nerve and its cross-sectional area, both of which are of particular relevance in CTS imaging. The field of view is usually set at 8 cm, and slice thickness is acquired between 2 and 3 mm [7, 9] (Figs. 8.4, 8.5, 8.6, and 8.7).

The median nerve contours seen on MRI are defined by its outermost connective tissue sheath, called the epineurium. A surrounding rim of epineural fat may be visible, appearing as a high-signal rim on PD- or T1-weighted images and low signal on fat-suppressed imaging. High-resolution imaging may also depict the individual nerve fascicles, which should demonstrate intermediate signal slightly higher than that of the normal muscle. The loss of the normal internal fascicular architecture of the nerve coupled with high signal within the nerve is an abnormal finding, suggesting edema or neuritis. Segmental or diffuse enlargement of the nerve is also commonly seen with neuritis. When the median nerve demonstrates focal or fusiform thickening, one should assess for a possible neoplasm or posttraumatic neuroma [9, 10].

On fast spin-echo PD- and T2-weighted sequences, the normal muscle is intermediate-signal intensity. Acutely denervated, muscle tissue will demonstrate abnormal MRI signal that precedes actual muscle volume loss and atrophy. This abnormal signal or prolonged T2 relaxation time is hyperintense (bright) on PD- and T2-weighted sequences. This change is thought to be due to fluid movement from the intracellular space into the extracellular space as well as capsular engorgement and increased muscle blood volume [7, 11, 12]. The chronic findings of muscle atrophy and fat replacement are also well depicted on fast spin-echo PD- or even better on T1-weighted sequences, as fat is bright or hyperintense on these sequences.

On a conventional wrist MRI, there are four general categories of imaging findings in carpal tunnel syndrome: increased median nerve size, median nerve flattening, median nerve signal change, and flexor retinaculum bowing. Each of these criteria has varied sensitivities and specificities for CTS when evaluated individually. However, when combined as an overall impression, MRI has a sensitivity as high as 96% but a low specificity (33%) [13].

Median Nerve Enlargement

Patients with carpal tunnel syndrome can often have median nerve enlargement (Fig. 8.8). This is most objectively assessed by measuring the cross-sectional area of the nerve on an axial image. In the literature, three levels within the wrist have been most commonly used as landmarks for measurement: (1) distal radioulnar joint (DRUJ), (2) pisiform, and (3) hamate.

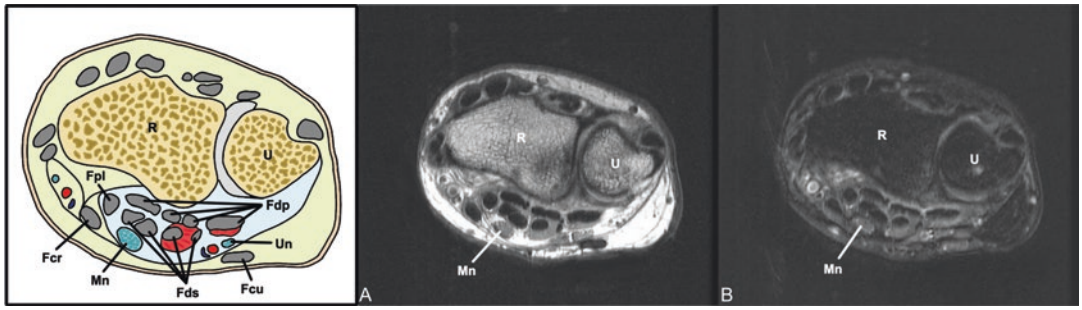

Fig. 8.4 Axial MRI proton density (**a**) and T2 fat saturation (**b**)—normal anatomy at the level of the DRUJ; *R* radius, *U* ulna, *Mn* median nerve, *Un* ulnar nerve, *Fdp* flexor digitorum profundus, *Fds* flexor digitorum superficialis, *Fpl* flexor pollicis longus, *Fcr* flexor carpi radialis, *Fcu* flexor carpi ulnaris

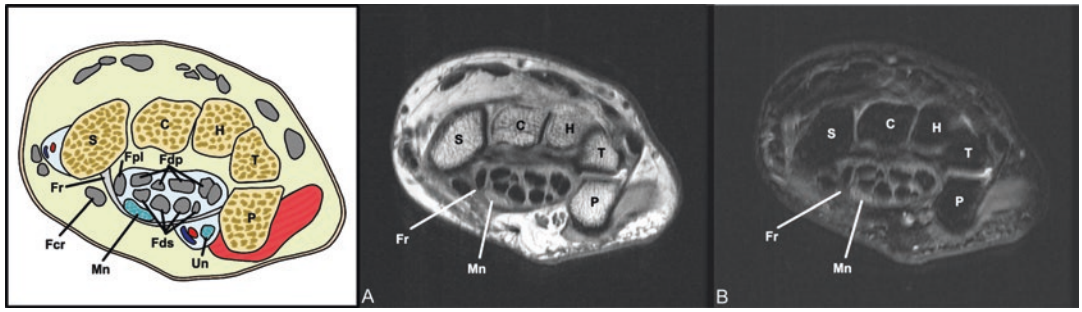

Fig. 8.5 Axial MRI proton density (**a**) and T2 fat saturation (**b**)—normal anatomy at the level of the pisiform; *S* scaphoid, *C* capitate, *H* hamate, *T* triquetrum, *P* pisiform, *Mn* median nerve, *Un* ulnar nerve, *Fdp* flexor digitorum profundus, *Fds* flexor digitorum superficialis, *Fpl* flexor pollicis longus, *Fcr* flexor carpi radialis, *Fcu* flexor carpi ulnaris, *Fr* flexor retinaculum

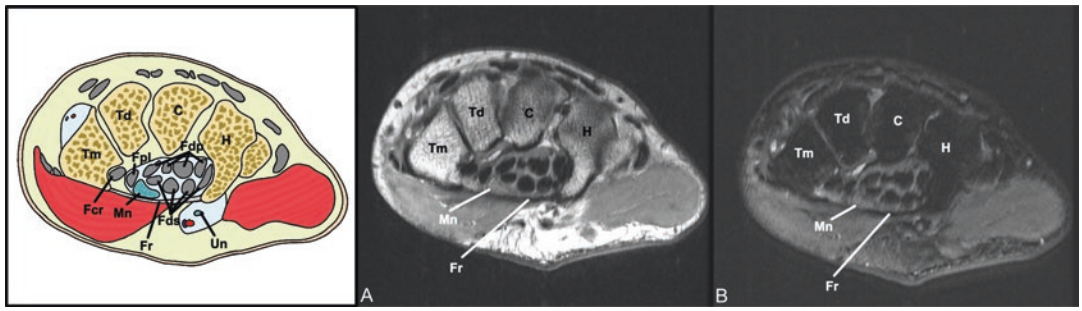

Fig. 8.6 Axial MRI proton density (**a**) and T2 fat saturation (**b**)—normal anatomy at the level of the hamate; *Tm* trapezium, *Td* trapezoid, *C* capitate, *H* hamate, *Mn* median nerve, *Un* ulnar nerve, *Fdp* flexor digitorum profundus, *Fds* flexor digitorum superficialis, *Fpl* flexor pollicis longus, *Fcr* flexor carpi radialis, *Fr* flexor retinaculum

Absolute cutoff values for the normal median cross-sectional area have varied between studies, some with less than desirable reproducibility [14]. A more useful and reproducible reference standard for CTS is the ratio of the surface area of the median nerve at the level of the pisiform relative to the median nerve surface area at the DRUJ. Quantitative analysis

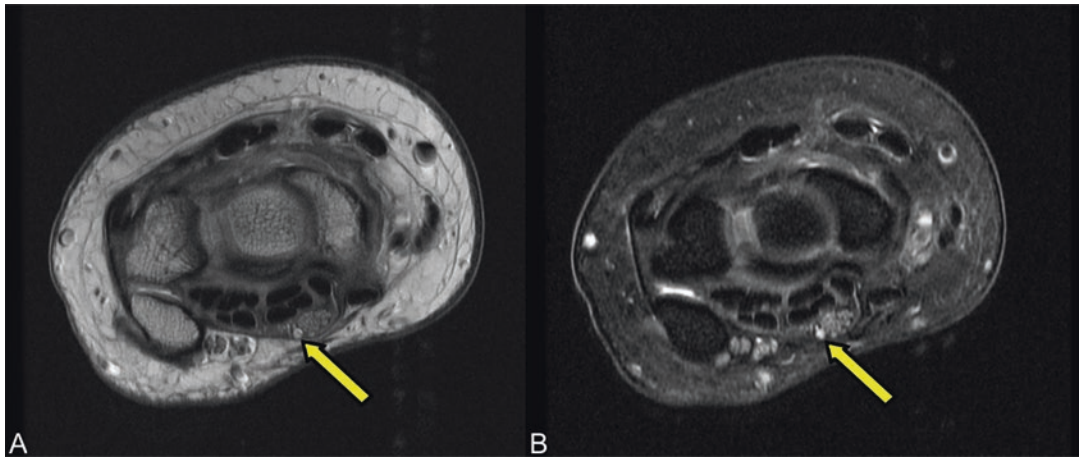

Fig. 8.7 Axial MRI proton density (**a**) and T2 fat saturation (**b**) at the level of the pisiform—median nerve enlargement and high signal with variant vascular anatomy; persistent median artery (*yellow arrow*)

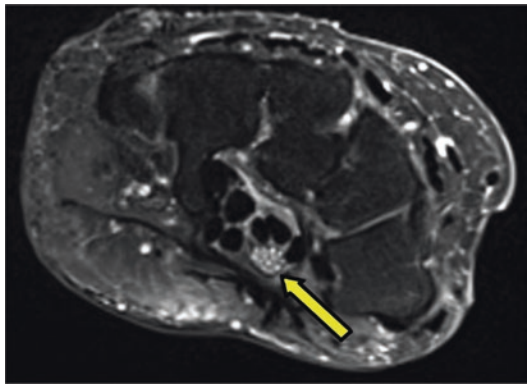

Fig. 8.8 Axial MRI T2 fat saturation—median nerve enlargement with high internal signal (*yellow arrow*) and bowing of the flexor retinaculum

has shown that in normal asymptomatic subjects, the mean pisiform/DRUJ ratio is 1.1. In patients with CTS, the mean pisiform/DRUJ ratio is as high as 2.4 [15]. While the mean cross-sectional area ratio can also be taken at the level of the hamate, the difference between normal and CTS is not as large. Careful measurements of the median nerve cross-sectional area can be time-consuming, and an effective method for determining median nerve enlargement is finding a nerve that is 2–3 times larger at the pisiform than at the DRUJ.

Median Nerve Flattening

The median nerve normally undergoes a small degree of flattening within the carpal tunnel; however, excessive nerve flattening can indicate CTS. As this observation can be subjective, a flattening ratio can be a more effective means of quantitatively determining the severity. The ratio is made by measuring the major and minor axes of the nerve at the level of the DRUJ as well as within the carpal tunnel. In patients with CTS, the mean flattening ratio at the DRUJ is 1.8 at the distal radius, but increases up to 3.8 at the level of the hamate [12, 15]. Thus, a median nerve that is 3–4 times wide as it is thick is associated with CTS (Fig. 8.9).

Flexor Retinaculum Bowing

Normally, the flexor retinaculum is flat or convex at the level of the hamate, where thickness is the greatest. In CTS, a bowed flexor retinaculum implies median nerve compression. The degree of bowing can be quantified by dividing the distance of palmar displacement of the retinaculum by the distance between the hook of the hamate and the tubercle of the trapezium. In normal patients, the ratio ranges from 0 to 0.15. In

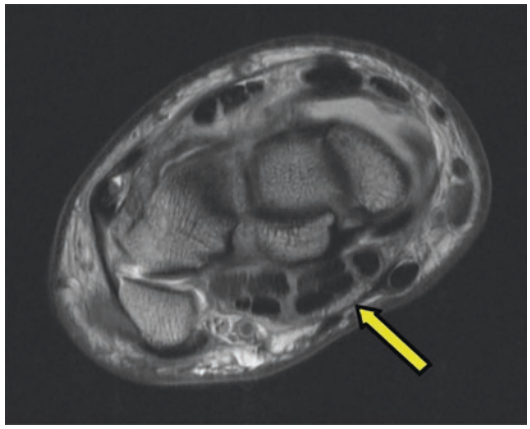

Fig. 8.9 Axial MRI PD—flattening of the median nerve (*yellow arrow*) at the level of the pisiform

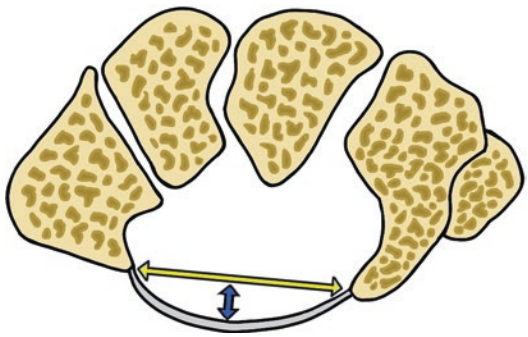

Fig. 8.10 Flexor retinacular bowing ratio—distance of palmar displacement (*blue arrow*) divided by the distance between the hamate hook and trapezium (*yellow arrow*)

patients with carpal tunnel syndrome, this ratio is between 0.14 and 0.26 [15] (Fig. 8.10).

Hyperintense Median Nerve Signal

Normally, the median nerve will have an internal signal similar to or slightly higher than that of muscle tissue on fast spin-echo PD- and T2-weighted sequences. The signal is generally uniform throughout the length of the nerve within the field of view. When the median nerve is bright or high signal on these sequences, the finding is highly sensitive for CTS (88%). This finding however should be treated with caution, as it is unfortunately low in specificity (39%) [13]. The hypothesized pathophysiology for abnormal signal of the nerve may be related to localized edema signal or fluid accumulation within the endoneural spaces [9]. On routine MRI sequencing of the wrist, this finding is made by visual inspection; no reliable quantitative measuring system is accepted. Despite the potential for subjectivity, studies have shown at least substantial inter-reader agreement (weighted kappa = 0.71) when judging median nerve signal abnormality [13] (Fig. 8.11).

Additional MRI Findings

Thenar muscle denervation effect on MRI is indicated by high signal on either PD- or T2-weighted fat-suppressed imaging. This finding is not particularly sensitive for CTS (10%) but is highly specific (96%) (Fig. 8.12) and considered a late-stage finding, correlating with clinically severe CTS and high-grade denervation by EDT [10].

When mechanical compression is the cause of CTS, there are many pathologic lesions that can be discovered by MRI. Flexor tenosynovitis due to infectious or inflammatory arthropathy (such as rheumatoid arthritis or gout) or nonspecific repetitive motion can be indicated by the high fluid signal and distension outlining the flexor tendons on either PD- or T2-weighted sequences (Fig. 8.13). Space-occupying lesions such as ganglion cysts or neoplastic lesions can also be implicated in nerve compression. If a neurogenic tumor or sarcomatous lesion is suspected, MRI protocols that are further optimized for soft tissue imaging may be needed for characterization. This includes the use of pre- and post-intravenous contrast T1-weighted fat-suppressed sequences which can further grade the lesion margins and its overall vascularity and enhancement [16] (Fig. 8.14).

Postsurgical MR Imaging

MRI can be helpful in evaluating the causes of recurrent CTS after surgical release. Similar to pretreatment imaging, the findings have varied sensitivities and specificities and should be combined with EDT findings. In addition to the routine axial wrist sequences, pre- and post-intravenous

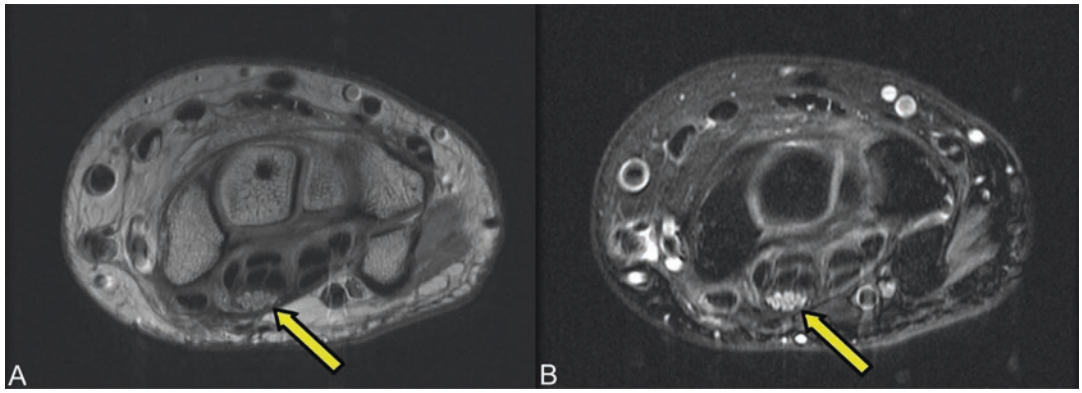

Fig. 8.11 Axial MRI proton density (**a**) and T2 fat saturation (**b**) at the level of the pisiform—median nerve enlargement and high-signal intensity (*yellow arrow*)

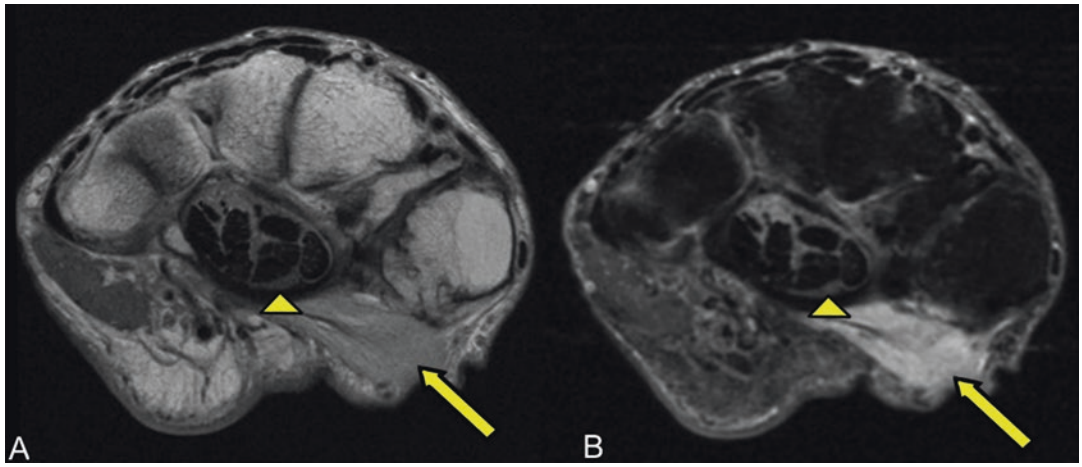

Fig. 8.12 Axial MRI proton density (**a**) and T2 fat saturation (**b**)—muscle atrophy and denervation high signal within the thenar muscles (opponens pollicis and abductor pollicis brevis, *yellow arrow*). The median nerve is flattened within the carpal tunnel (*arrowhead*)

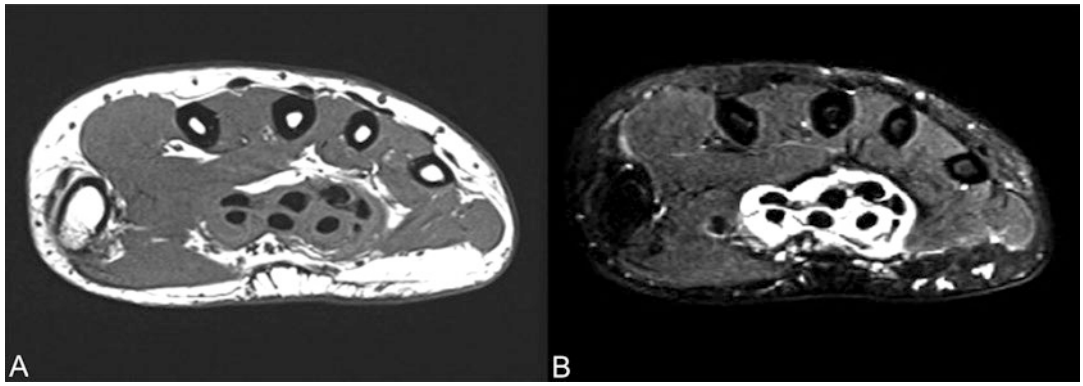

Fig. 8.13 Axial MRI T1 (**a**) and T2 fat saturation (**b**)—tenosynovitis of the flexor tendons in rheumatoid arthritis

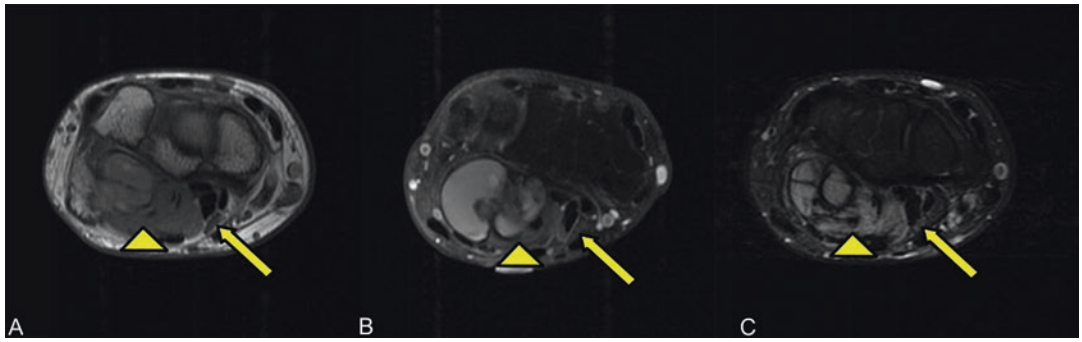

Fig. 8.14 Axial MRI T1 (**a**), T2 fat saturation (**b**), and T1 fat saturation post IV contrast (**c**)—synovial sarcoma within the carpal tunnel; T2 hyperintense, enhancing mass (*arrowhead*) that is displacing and flattening the median nerve (*yellow arrow*)

contrast T1-weighted fat-suppressed sequences are recommended to evaluate the postoperative changes. The aforementioned routine MRI criteria of CTS remain helpful in the assessment of the postoperative wrist. Of these findings, an increased flattening ratio is the most statistically significant difference between EDT-confirmed recurrent CTS and postoperative controls [17].

Additional statistically significant changes in the postoperative patient with recurrent CTS include the presence of perineural fibrosis, median nerve enhancement, and insufficient release of the tunnel. Fibrosis appears as extensive low-signal intensity with an ill-defined nerve margin on either nonfat-suppressed PD- or T1-weighted fast spin-echo sequences. Fibrosis is 60% sensitive, but 83% specific for recurrent CTS. Median nerve enhancement after intravenous contrast administration is considered present if the signal is higher than the level of enhancement of the thenar muscle. While not highly sensitive (40%), this is highly specific (92%) for recurrent CTS [17].

Findings indicating insufficient carpal tunnel decompression have the highest relative sensitivity for recurrent CTS in the postoperative patient population (80%). This is assessed by determining the position of the median nerve and leading flexor tendon, relative to a line joining the hook of the hamate to the ridge of the trapezium. Volar migration of the median nerve and tendon beyond this line can be considered a successful decompression. Other MRI findings such as regrowth of the flexor retinaculum, cross-sectional area of the nerve, and nerve signal intensity on T2-weighted images have not been found to be statistically significant [17] (Fig. 8.15).

Advanced MRI Techniques

Diffusion tensor imaging (DTI) is an advanced MRI technique based on the natural free diffusion of water molecules. While in free fluid, this movement can occur in any random direction. In a highly organized tissue, such as a myelinated nerve, this movement is restricted and occurs along the direction of the nerve. Abnormalities of the mean diffusivity and the direction of this diffusion reflect nerve damage and can be assessed quantitatively by using the imaging to create parameters such as apparent diffusion coefficient (ADC) and fractional anisotropy (FA). The imaging data can further be used to perform tractography, which creates a 3D image of the orientation and course of the nerves [6, 14, 18–20].

Patients with CTS have demonstrated statistically significant decreasing FA and increased ADC values compared to normal asymptomatic patients. These changes reflect a general trend of the diffusion within the nerve toward randomness, indicating nerve pathology [21–23]. Pilot studies have recently used DTI to evaluate CTS patients before and after carpal tunnel release. Naraghi et al. were

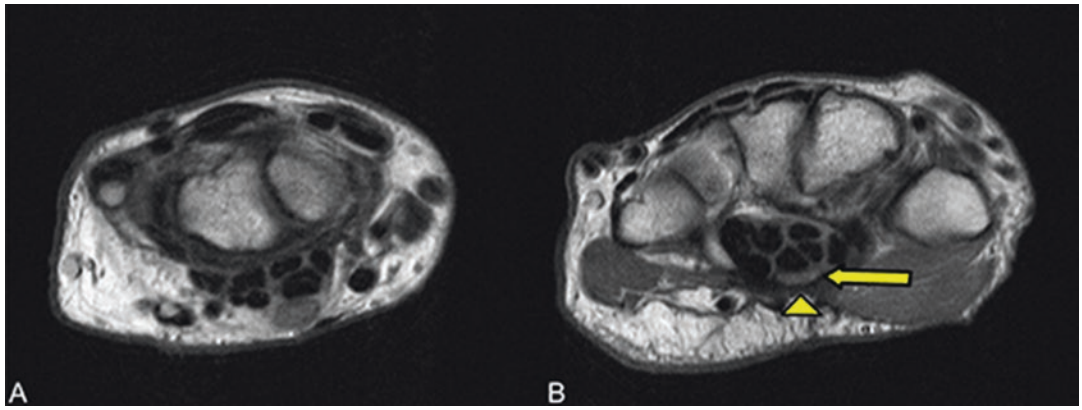

Fig. 8.15 Axial MRI T1 images at the DRUJ (**a**) and hamate (**b**)—status post carpal tunnel release with return of symptoms; residual scarring and insufficient decompression of the flexor retinaculum (*arrowhead*) and a persistently flattened median nerve (*yellow arrow*)

able to show a significant increase in FA and a decrease in ADC values associated with improvement in symptoms after decompression surgery, indicating that these diffusion changes are reversible [24]. Future studies will determine the sensitivities and specificities of DTI relative to the more commonly used MRI findings of CTS. Additionally, as normal diffusion values can vary depending on anatomic location and age, further work is needed to define normal and abnormal threshold values [25].

Ultrasound

Ultrasound has emerged as an important diagnostic tool in CTS. The superficial location of the carpal tunnel and median nerve allow diagnostic evaluation, creating images that are high in spatial resolution and image contrast, but without ionizing radiation. When using the Carpal Tunnel Syndrome 6 (CTS-6) clinical diagnostic tool as the reference standard, ultrasound has a sensitivity of 89% and a specificity of up to 90%, which is similar to EDT's sensitivity (89%) and specificity (80%) [1]. In addition, ultrasound is a relatively inexpensive, noninvasive test that has been shown to be a cost-effective alternative to EDT [26, 27].

Ultrasound Technique

Proper technique and a basic understanding of ultrasound imaging are essential in carpal tunnel imaging. A high-frequency transducer of at least 10 MHz is typically used. The patient is seated with the arm extended and the forearm supinated. The wrist should be rested on a hard flat surface and the fingers can be semi-extended. Images are obtained in both the axial and sagittal plane. Like MRI, the axial plane is the most useful for diagnostic criteria. In addition to the bony landmarks used on MRI (pisiform and hamate hook), the median nerve should be evaluated both immediately proximal to the carpal tunnel and at the carpal tunnel inlet which is defined at a level immediately deep to the proximal edge of the flexor retinaculum [27] (Figs. 8.16, 8.17, and 8.18).

An ultrasound image is produced when high-frequency sound waves emitted by the transducer interact with tissue. Depending on the tissue interfaces and impedance, the sound waves are reflected at different intensities. A strong reflection produces a "hyperechoic" signal that is bright on screen. A particularly strong reflection that can occur at bony interfaces will also produce a "shadowing" effect of any structures beyond the interface. An area that does not produce any echo is termed "anechoic" and thus will be black

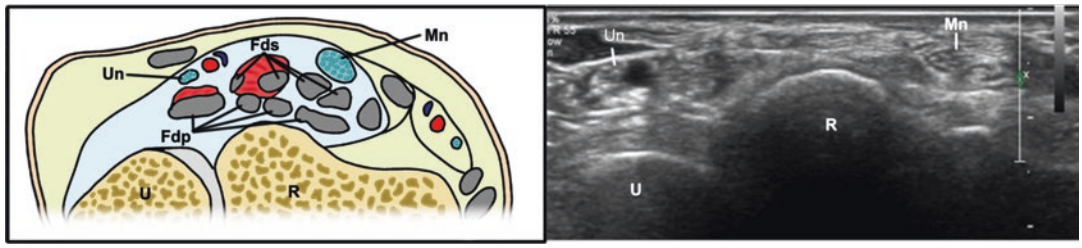

Fig. 8.16 Axial ultrasound image—normal anatomy at the DRUJ; *R* radius, *U* ulna, *Mn* median nerve, *Un* ulnar nerve, *Fdp* flexor digitorum profundus, *Fds* flexor digitorum superficialis

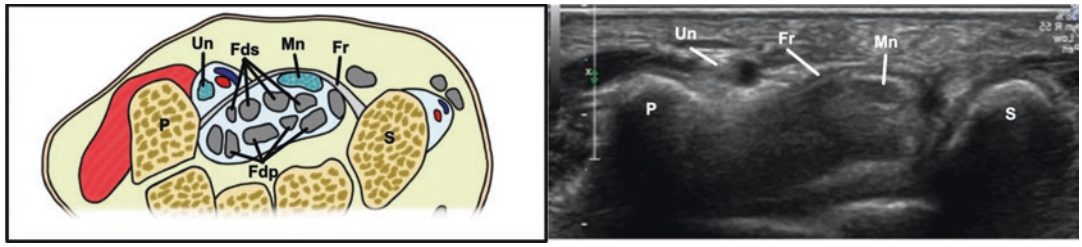

Fig. 8.17 Axial ultrasound image—normal anatomy at the pisiform; *S* scaphoid, *C* capitate, *H* hamate, *T* triquetrum, *P* pisiform, *Mn* median nerve, *Un* ulnar nerve, *Fdp* flexor digitorum profundus, *Fds* flexor digitorum superficialis, *Fr* flexor retinaculum

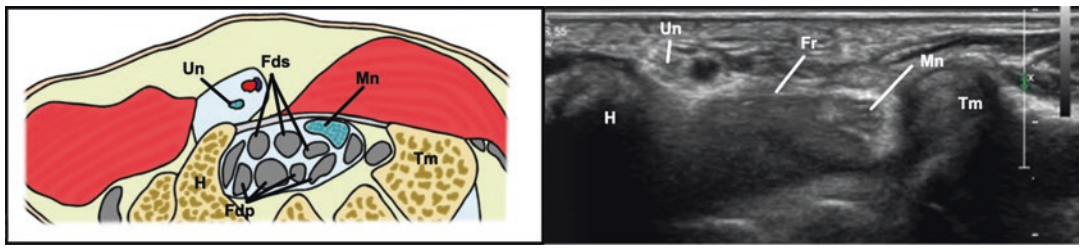

Fig. 8.18 Axial ultrasound image—normal anatomy at the hamate hook; *Tm* trapezium, *Td* trapezoid, *C* capitate, *H* hamate, *Mn* median nerve, *Un* ulnar nerve, *Fdp* flexor digitorum profundus, *Fds* flexor digitorum superficialis, *Fpl* flexor pollicis longus, *Fcr* flexor carpi radialis, *Fcu* flexor carpi ulnaris, *Fr* flexor retinaculum

on the screen. An area with a weak or low reflection is termed "hypoechoic" and is dark on the screen [28]. Normal tendons are hyperechoic or bright on ultrasound, and the fibrillar-like architecture of the longitudinal tendon fibers is well depicted. A confounding artifact is "anisotropy." When a fibrillar structure like a tendon is imaged at a plane that is angled as little as 5° perpendicular to the probe, the structure can lose its hyperechoic appearance and appear artificially hypoechoic or dark.

The normal median nerve will have an internal fascicular pattern on ultrasound, characterized as a "honeycomb" appearance. The individual nerve fascicles will be hypoechoic or dark and outlined by hyperechoic connective tissue. Mass lesions within the carpal tunnel can have varied echogenicities based on internal composition (Fig. 8.19). Color and power Doppler settings on the ultrasound can be used to depict blood flow patterns that are superimposed on the baseline grayscale imaging [28]. Applying this color

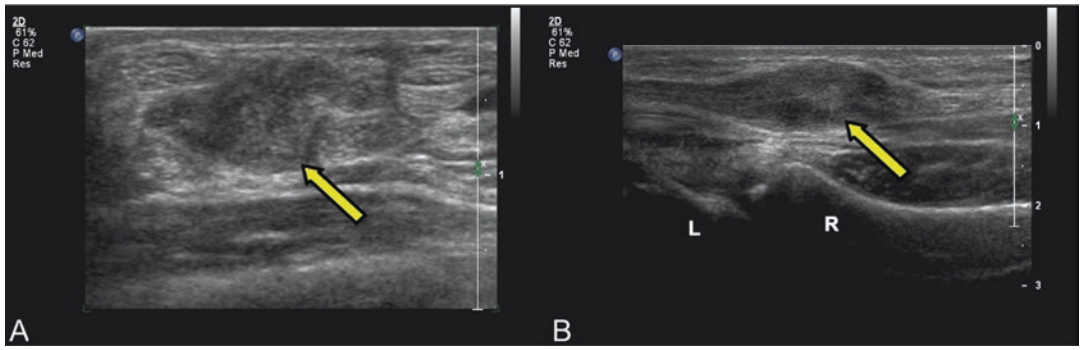

Fig. 8.19 Axial ultrasound image in the axial (**a**) and sagittal (**b**) planes—nerve sheath tumor of the median nerve (*yellow arrow*); *R* radius, *L* lunate

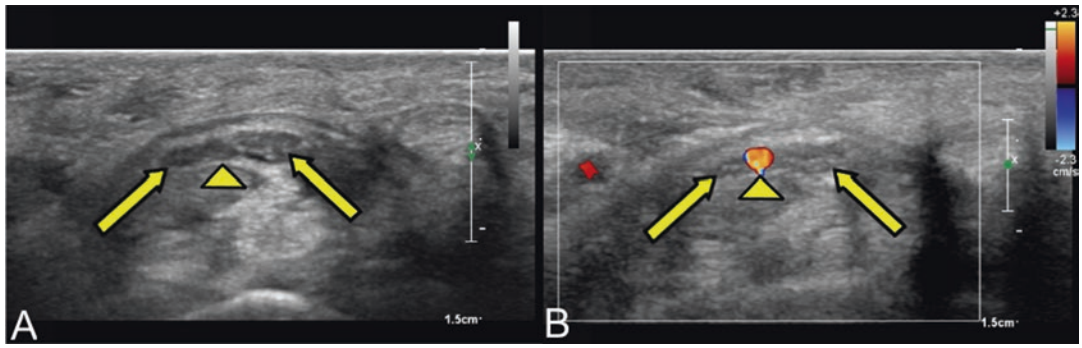

Fig. 8.20 Axial ultrasound image 2D gray scale (**a**) and color Doppler (**b**)—Bifid median nerve (*yellow arrow*) with persistent median artery (*arrowhead*)

Doppler setting is especially helpful in identifying vascular lesions, variant vascular anatomy, and tissue hyperemia (Fig. 8.20).

Although ultrasound of the carpal tunnel can depict similar MRI criteria used in CTS, the most commonly evaluated parameter has been the median nerve cross-sectional area. Using the circumferential trace mode on the ultrasound screen, the cross-sectional area of the median nerve can be measured. A widely accepted cutoff cross-sectional surface area for CTS with the highest sensitivity and specificity is 10 mm^2, measured at the carpal tunnel inlet or pisiform. This sensitivity and specificity is highly comparable to EDT [1, 27–30] (Fig. 8.21).

Other parameters unique to ultrasound can be supplemental to the cross-sectional measurement of the median nerve. In particular, color and power Doppler imaging can be used in the routine ultrasound examination to detect the presence of intraneural vascularity, which would indicate the presence of inflammatory changes within the nerve. While this phenomenon has been less studied than surface area measurements, studies have shown the sensitivity and specificity to be as high as 83% and 89%, respectively [31] (Fig. 8.22). Additional studies have observed restricted median nerve mobility in CTS, during passive flexion and extension of the digits [32]. This is thought to be due to fibrosis or adherence of the median nerve to the retinaculum. Real-time ultrasound allows for this dynamic evaluation. Subjective assessments of this restricted mobility have been shown to be specific (86%) with high interoperator reliability [33]. Since hyperemia, fibrosis, and median nerve-restricted movement

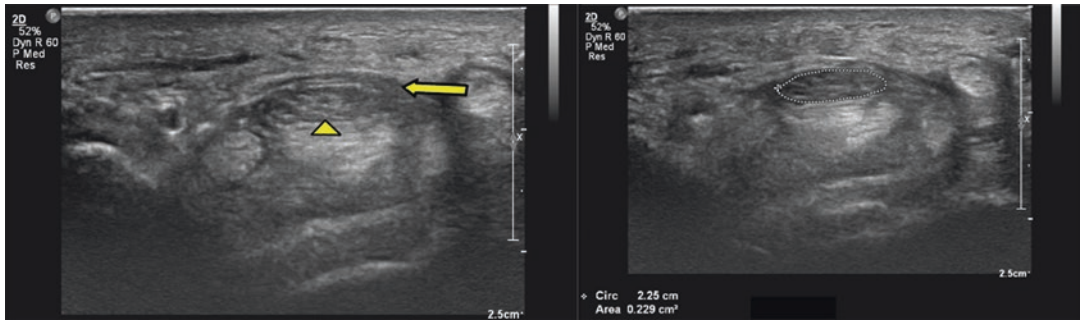

Fig. 8.21 Axial ultrasound image—median nerve enlargement (*arrowhead*) and flexor retinaculum thickening and bowing at the carpal tunnel inlet. The cross-sectional area >10 mm^2 is highly sensitive and specific for CTS

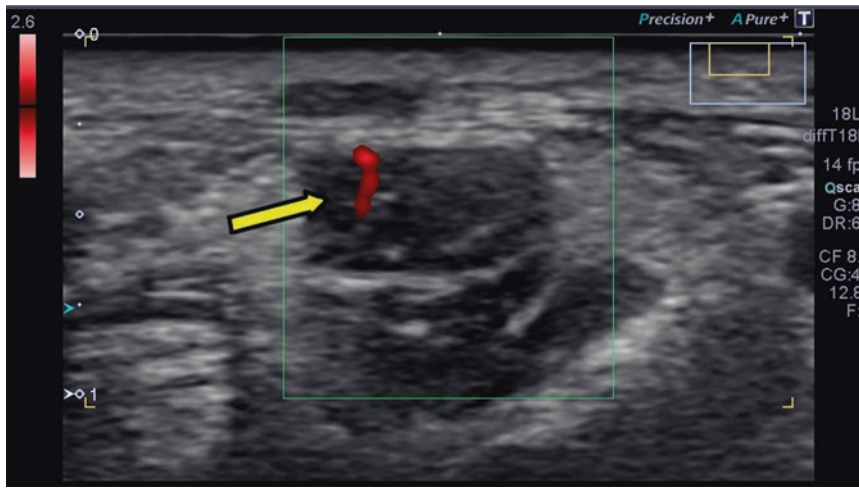

Fig. 8.22 Axial ultrasound image—median nerve enlargement with intraneural vascularity by color Doppler (*arrow*). *Image provided courtesy of Toshiba America Medical Systems, Inc.*

are likely later-stage findings of CTS, this may account for the relatively lower sensitivity of the ultrasound findings when compared to the cross-sectional area measurement. Despite this, when taken in combination with surface area, these findings can improve the sensitivity and accuracy of ultrasound.

Flexor retinacular bowing and median nerve flattening ratios are measured in a similar fashion as MRI. These parameters have been studied less than other ultrasound findings, but recent studies have demonstrated lesser sensitivities (63% and 44%), specificities (60% and 85%), and poor interobserver reliability [33]. This may be due to the technical challenges of evaluating the distal carpal tunnel and the oblique and changing course of the median nerve.

Postoperative Assessment

In the postoperative patient, the conventional ultrasound parameters of CTS can be used to assess treatment response. As the cross-sectional area of the median nerve has been found to decrease over a period of 4–12 weeks after surgical release, this measurement has particular importance [34]. Additional assessment of the flexor retinaculum and perineural fibrosis can also be made (Fig. 8.23).

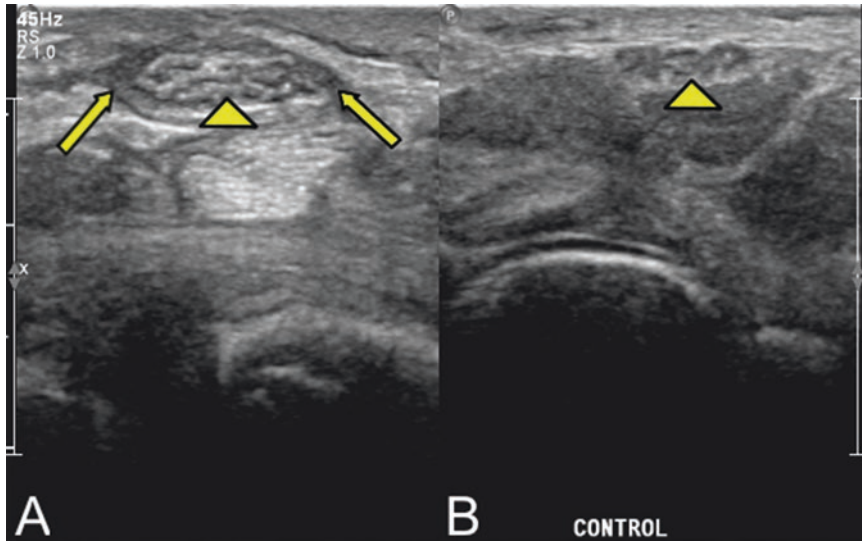

Fig. 8.23 Axial ultrasound image—postoperative patient with recurrent CTS symptoms. Note the relative enlargement of the nerve (*arrowhead*) and the surrounding scar tissue (*arrow*) about the nerve on the postoperative wrist on the left (**a**) relative to the contralateral asymptomatic wrist on the right (**b**)

Ultrasound Elastography: Emerging Ultrasound Technology

Ultrasound elastography is a method that allows the qualitative visual or quantitative measurement of soft tissue stiffness. By applying a low-frequency strain or compression, the mechanical properties of a selected tissue can be analyzed by its tendency to return to its original size and shape. In CTS, the focal demyelination and axonal degeneration can lead to a fibrotic response of the nerve. Additionally, there can be an increased carpal tunnel pressure in CTS. Both factors can create an overall stiffer nerve, which can be detected by ultrasound elastography. There are currently several elastography techniques such as strain elastography, acoustic radiation force impulse, transient elastography, and shear wave elastography. Each method has its strength and weakness. Strain elastography has been the most widely studied procedure for musculoskeletal applications. The degree of strain or elasticity is converted into a color-coded map that is superimposed on the traditional grayscale ultrasound image (Fig. 8.24). Early published reports suggest that strain elastography may have a sensitivity and specificity that is comparable to cross-sectional surface area measurements in the diagnosis of CTS. Further studies are needed to evaluate ultrasound elastography and its application in CTS; however, initial results are promising [35–38].

Conclusion

The current recommendations for the diagnosis of CTS have reiterated the importance of obtaining an accurate patient history and physical exam, as well as performing EDTs in the appropriate clinical scenarios [2]. Although radiologic imaging is not recommended for routine use, recent advancements in MRI and ultrasound have increased their importance. A variety of different imaging findings have been found in CTS with varied sensitivities and specificities and thus should be taken as a whole when evaluating this clinical diagnosis. In MRI, median nerve enlargement, nerve flattening, flexor retinacular bowing, and increased nerve signal are findings typical in CTS. While similar findings can be seen in ultrasound, cross-sectional area enlargement has demonstrated a particularly high sensitivity and specificity. Both ultrasound and MRI are also

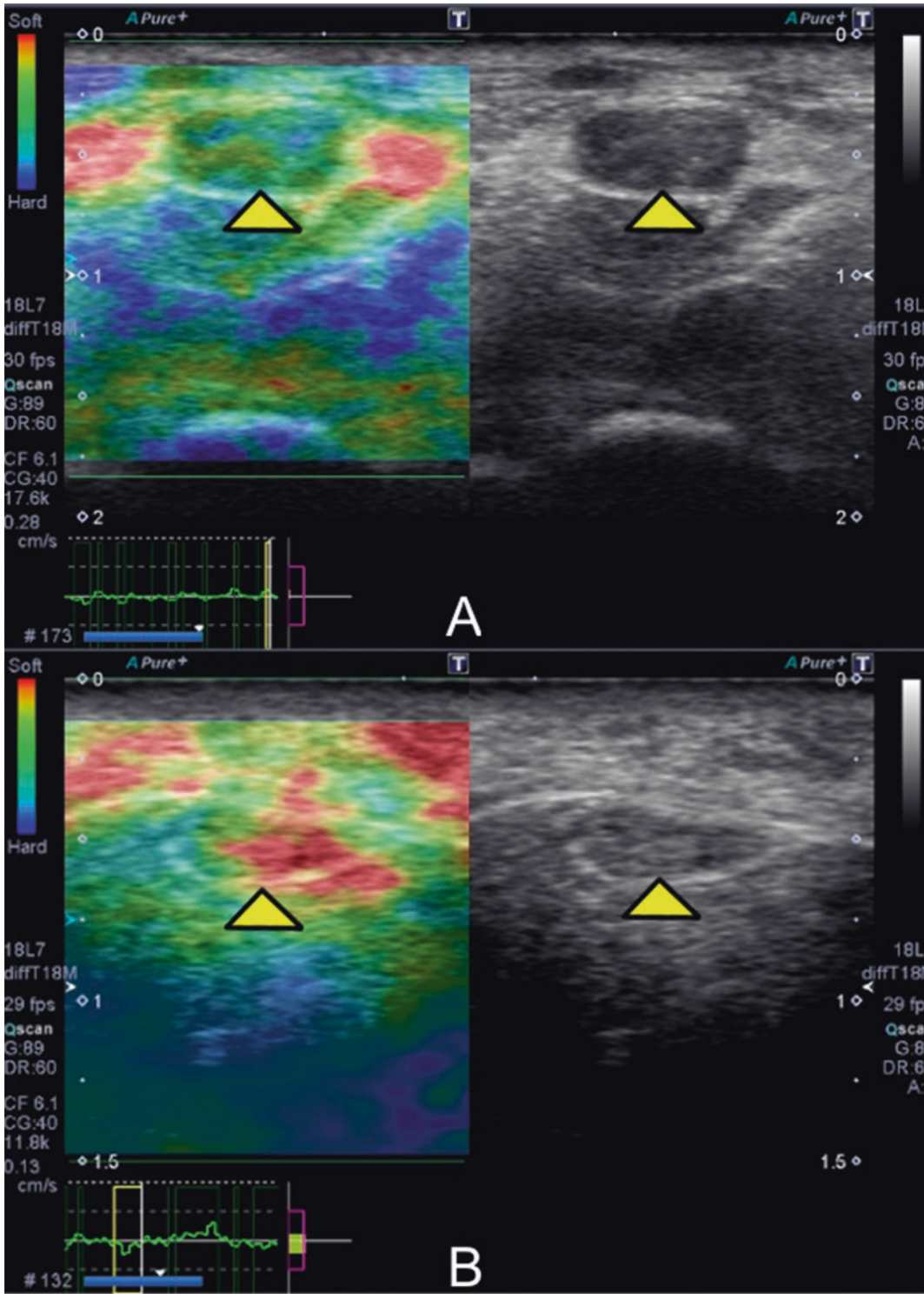

Fig. 8.24 Ultrasound strain elastography—CTS patient (**a**) with an enlarged median nerve (*arrowhead*) and color mapping on elastography indicating increased nerve stiffness (*blue*) compared to a normal asymptomatic patient (**b**) with a normal size median nerve (*arrowhead*) and color mapping on elastography indicating a soft (*red*) nerve. *Image provided courtesy of Toshiba America Medical Systems, Inc.*

helpful in identifying alternative causes of nerve compression, which include ganglion cysts, mass lesions, and infectious or inflammatory flexor tenosynovitis. Variant anatomy, which can affect surgical planning, can also be readily identified. Future research will continue to determine if there will be greater role of these modalities in the routine diagnostic evaluation.

References

1. Fowler JR, Munsch M, Tosti R, Hagberg WC, Imbriglia JE. Comparison of ultrasound and electrodiagnostic testing for diagnosis of carpal tunnel syndrome: study using a validated clinical tool as the reference standard. J Bone Joint Surg Am. 2014;96(17):e148.
2. Keith MW, Masear V, Chung KC, Maupin K, Andary M, Amadio PC, et al. American Academy of Orthopaedic Surgeons clinical practice guideline on diagnosis of carpal tunnel syndrome. J Bone Joint Surg Am. 2009;91(10):2478–9.
3. Keith MW, Masear V, Chung K, Maupin K, Andary M, Amadio PC, et al. Diagnosis of carpal tunnel syndrome. J Am Acad Orthop Surg. 2009;17(6):389–96.
4. Klauser AS, Halpern EJ, De Zordo T, Feuchtner GM, Arora R, Gruber J, et al. Carpal tunnel syndrome assessment with US: value of additional cross-sectional area measurements of the median nerve in patients versus healthy volunteers. Radiology. 2009;250(1):171–7.
5. Middleton WD, Kneeland JB, Kellman GM, Cates JD, Sanger JR, Jesmanowicz A, et al. MR imaging of the carpal tunnel: normal anatomy and preliminary findings in the carpal tunnel syndrome. AJR Am J Roentgenol. 1987;148(2):307–16.
6. Klauser AS, Faschingbauer R, Bauer T, Wick MC, Gabl M, Arora R, et al. Entrapment neuropathies II: carpal tunnel syndrome. Semin Musculoskelet Radiol. 2010;14(5):487–500.
7. Stoller DW, Li AE, Lichtman DM, Brody GA. The wrist and hand. In: Stoller DW, editor. Magnetic resonance imaging in orthopaedics and sports medicine. 3rd ed. Philadelphia: Lippincott Williams & Wilkins; 2007. p. 1627.
8. Javed S, Woodruff M. Carpal tunnel syndrome secondary to an accessory flexor digitorum superficialis muscle belly: case report and review of the literature. Hand (N Y). 2014;9(4):554–5.
9. Maravilla KR, Bowen BC. Imaging of the peripheral nervous system: evaluation of peripheral neuropathy and plexopathy. AJNR Am J Neuroradiol. 1998;19(6):1011–23.
10. Britz GW, Haynor DR, Kuntz C, Goodkin R, Gitter A, Kliot M. Carpal tunnel syndrome: correlation of magnetic resonance imaging, clinical, electrodiagnostic, and intraoperative findings. Neurosurgery. 1995;37(6):1097–103.
11. Bendszus M, Koltzenburg M, Wessig C, Solymosi L. Sequential MR imaging of denervated muscle: experimental study. AJNR Am J Neuroradiol. 2002;23(8):1427–31.
12. Stoller DW, Li AE, Lichtman DM, Brody GA. Entrapment neuropathies of the upper extremity. In: Stoller DW, editor. Magnetic resonance imaging in orthopaedics and sports medicine. 3rd ed. Philadelphia: Lippincott Williams & Wilkins; 2007. p. 1933.
13. Jarvik JG, Yuen E, Haynor DR, Bradley CM, Fulton-Kehoe D, Smith-Weller T, et al. MR nerve imaging in a prospective cohort of patients with suspected carpal tunnel syndrome. Neurology. 2002;58(11):1597–602.
14. Yao L, Gai N. Median nerve cross-sectional area and MRI diffusion characteristics: normative values at the carpal tunnel. Skelet Radiol. 2009;38(4):355–61.
15. Mesgarzadeh M, Schneck CD, Bonakdarpour A, Mitra A, Conaway D. Carpal tunnel: MR imaging. Part II. Carpal tunnel syndrome. Radiology. 1989;171(3):749–54.
16. Wu JS, Hochman MG. Soft-tissue tumors and tumor-like lesions: a systematic imaging approach. Radiology. 2009;253(2):297–316.
17. Campagna R, Pessis E, Feydy A, Guerini H, Le Viet D, Corlobe P, et al. MRI assessment of recurrent carpal tunnel syndrome after open surgical release of the median nerve. AJR Am J Roentgenol. 2009;193(3):644–50.
18. Sasiadek MJ, Szewczyk P, Bladowska J. Application of diffusion tensor imaging (DTI) in pathological changes of the spinal cord. Med Sci Monit. 2012;18(6):RA73–9.
19. Jambawalikar S, Baum J, Button T, Li H, Geronimo V, Gould ES. Diffusion tensor imaging of peripheral nerves. Skelet Radiol. 2010;39(11):1073–9.
20. Hiltunen J, Suortti T, Arvela S, Seppa M, Joensuu R, Hari R. Diffusion tensor imaging and tractography of distal peripheral nerves at 3 T. Clin Neurophysiol. 2005;116(10):2315–23.
21. Stein D, Neufeld A, Pasternak O, Graif M, Patish H, Schwimmer E, et al. Diffusion tensor imaging of the median nerve in healthy and carpal tunnel syndrome subjects. J Magn Reson Imaging. 2009;29(3):657–62.
22. Kabakci N, Gurses B, Firat Z, Bayram A, Ulug AM, Kovanlikaya A, et al. Diffusion tensor imaging and tractography of median nerve: normative diffusion values. AJR Am J Roentgenol. 2007;189(4):923–7.
23. Khalil C, Hancart C, Le Thuc V, Chantelot C, Chechin D, Cotten A. Diffusion tensor imaging and tractography of the median nerve in carpal tunnel syndrome: preliminary results. Eur Radiol. 2008;18(10):2283–91.
24. Naraghi A, da Gama LL, Menezes R, Khanna M, Sussman M, Anastakis D, et al. Diffusion tensor imaging of the median nerve before and after carpal tunnel release in patients with carpal tunnel syndrome: feasibility study. Skelet Radiol. 2013;42(10):1403–12.
25. Guggenberger R, Markovic D, Eppenberger P, Chhabra A, Schiller A, Nanz D, et al. Assessment of median nerve with MR neurography by using

diffusion-tensor imaging: normative and pathologic diffusion values. Radiology. 2012;265(1):194–203.
26. Fowler JR, Maltenfort MG, Ilyas AM. Ultrasound as a first-line test in the diagnosis of carpal tunnel syndrome: a cost-effectiveness analysis. Clin Orthop Relat Res. 2013;471(3):932–7.
27. Wong SM, Griffith JF, Hui AC, Lo SK, Fu M, Wong KS. Carpal tunnel syndrome: diagnostic usefulness of sonography. Radiology. 2004;232(1):93–9.
28. Jacobson JA. Fundamentals of musculoskeletal ultrasound. 1st ed. Philadelphia: Saunders; 2007.
29. Fowler JR, Gaughan JP, Ilyas AM. The sensitivity and specificity of ultrasound for the diagnosis of carpal tunnel syndrome: a meta-analysis. Clin Orthop Relat Res. 2011;469(4):1089–94.
30. Sernik RA, Abicalaf CA, Pimentel BF, Braga-Baiak A, Braga L, Cerri GG. Ultrasound features of carpal tunnel syndrome: a prospective case-control study. Skelet Radiol. 2008;37(1):49–53.
31. Ghasemi-Esfe AR, Khalilzadeh O, Vaziri-Bozorg SM, Jajroudi M, Shakiba M, Mazloumi M, et al. Color and power Doppler US for diagnosing carpal tunnel syndrome and determining its severity: a quantitative image processing method. Radiology. 2011;261(2):499–506.
32. Nakamichi K, Tachibana S. Restricted motion of the median nerve in carpal tunnel syndrome. J Hand Surg Br. 1995;20(4):460–4.
33. Ooi CC, Wong SK, Tan AB, Chin AY, Abu Bakar R, Goh SY, et al. Diagnostic criteria of carpal tunnel syndrome using high-resolution ultrasonography: correlation with nerve conduction studies. Skelet Radiol. 2014;43(10):1387–94.
34. Abicalaf CA, de Barros N, Sernik RA, Pimentel BF, Braga-Baiak A, Braga L, et al. Ultrasound evaluation of patients with carpal tunnel syndrome before and after endoscopic release of the transverse carpal ligament. Clin Radiol. 2007;62(9):891–4. discussion 895-6
35. Drakonaki EE, Allen GM, Wilson DJ. Ultrasound elastography for musculoskeletal applications. Br J Radiol. 2012;85(1019):1435–45.
36. Kantarci F, Ustabasioglu FE, Delil S, Olgun DC, Korkmazer B, Dikici AS, et al. Median nerve stiffness measurement by shear wave elastography: a potential sonographic method in the diagnosis of carpal tunnel syndrome. Eur Radiol. 2014;24(2):434–40.
37. Miyamoto H, Halpern EJ, Kastlunger M, Gabl M, Arora R, Bellmann-Weiler R, et al. Carpal tunnel syndrome: diagnosis by means of median nerve elasticity – improved diagnostic accuracy of US with sonoelastography. Radiology. 2014;270(2):481–6.
38. Klauser AS, Miyamoto H, Bellmann-Weiler R, Feuchtner GM, Wick MC, Jaschke WR. Sonoelastography: musculoskeletal applications. Radiology. 2014;272(3):622–33.